PAPER • **OPEN ACCESS**

An effective formaldehyde gas sensor based on oxygen-rich three-dimensional graphene

To cite this article: Shu Zhang *et al* 2022 *Nanotechnology* **33** 185702

OPEN ACCESS
IOP Publishing
Nanotechnology

Nanotechnology **33** (2022) 185702 (12pp) https://doi.org/10.1088/1361-6528/ac4eb4

An effective formaldehyde gas sensor based on oxygen-rich three-dimensional graphene

Shu Zhang[1,2,17], Jinbo Pang[1,17,*], Yufen Li[1,17], Bergoi Ibarlucea[3,4,17], Yu Liu[5,6], Ting Wang[7,8], Xiaoyan Liu[1], Songang Peng[9,10], Thomas Gemming[11], Qilin Cheng[1], Hong Liu[1,12,*], Jiali Yang[1], Gianaurelio Cuniberti[3,4,13,14,*], Weijia Zhou[1] and Mark H Rümmeli[5,6,11,15,16,*]

[1] Collaborative Innovation Center of Technology and Equipment for Biological Diagnosis and Therapy in Universities of Shandong, Institute for Advanced Interdisciplinary Research (iAIR), University of Jinan, Shandong, Jinan 250022, People's Republic of China
[2] School of Chemistry and Chemical Engineering, University of Jinan, Jinan, Shandong, Jinan 250022, People's Republic of China
[3] Institute for Materials Science and Max Bergmann Center of Biomaterials, Technische Universität Dresden, Dresden D-01069, Germany
[4] Center for Advancing Electronics Dresden, Technische Universität Dresden, Dresden D-01069, Germany
[5] College of Energy, Soochow Institute for Energy and Materials Innovations, Soochow University, Suzhou 215006, People's Republic of China
[6] Key Laboratory of Advanced Carbon Materials and Wearable Energy Technologies of Jiangsu Province, Soochow University, Suzhou 215006, People's Republic of China
[7] State Key Laboratory of Biobased Material and Green Papermaking, Qilu University of Technology, Shandong Academy of Sciences, No.3501 Daxue Road, Jinan 250353, People's Republic of China
[8] School of Bioengineering, Qilu University of Technology, Shandong Academy of Science, Jinan 250353, People's Republic of China
[9] High-Frequency High-Voltage Device and Integrated Circuits R&D Center, Institute of Microelectronics, Chinese Academy of Sciences, Beijing, 100029, People's Republic of China
[10] Key Laboratory of Microelectronic Devices & Integrated Technology, Institute of Microelectronics, Chinese Academy of Sciences, Beijing, 100029, People's Republic of China
[11] Institute for Complex Materials, Leibniz Institute for Solid State and Materials Research Dresden, PO Box 270116, Dresden, D-01171 Germany
[12] State Key Laboratory of Crystal Materials, Center of Bio & Micro/Nano Functional Materials, Shandong University, 27 Shandanan Road, Jinan 250100, People's Republic of China
[13] Dresden Center for Computational Materials Science, Technische Universität Dresden, Dresden D-01062, Germany
[14] Dresden Center for Intelligent Materials (GCL DCIM), Technische Universität Dresden, Dresden D-01062, Germany
[15] Centre of Polymer and Carbon Materials, Polish Academy of Sciences, M. Curie Sklodowskiej 34, Zabrze 41-819, Poland
[16] Institute of Environmental Technology (CEET), VŠB-Technical University of Ostrava, 17. Listopadu 15, Ostrava 708 33, Czech Republic

E-mail: ifc_pangjb@ujn.edu.cn, hongliu@sdu.edu.cn, gianaurelio.cuniberti@tu-dresden.de and m.ruemmeli@ifw-dresden.de

Received 15 December 2021, revised 20 January 2022
Accepted for publication 24 January 2022
Published 10 February 2022

[17] These authors contributed equally.
[*] Authors to whom any correspondence should be addressed.

Abstract

Three-dimensional (3D) graphene with a high specific surface area and excellent electrical conductivity holds extraordinary potential for molecular gas sensing. Gas molecules adsorbed onto graphene serve as electron donors, leading to an increase in conductivity. However, several challenges remain for 3D graphene-based gas sensors, such as slow response and long recovery time. Therefore, research interest remains in the promotion of the sensitivity of molecular gas detection. In this study, we fabricate oxygen plasma-treated 3D graphene for the high-performance gas sensing of formaldehyde. We synthesize large-area, high-quality, 3D graphene over Ni foam by chemical vapor deposition and obtain freestanding 3D graphene foam after Ni etching. We compare three types of strategies—non-treatment, oxygen plasma, and etching in HNO_3 solution—for the posttreatment of 3D graphene. Eventually, the strategy for oxygen plasma-treated 3D graphene exceeds expectations, which may highlight the general gas sensing based on chemiresistors.

Supplementary material for this article is available online

Keywords: 3D graphene, chemical vapor deposition, chemiresistors, oxygen plasma treatments, gas sensing

Introduction

Graphene is an ideal two-dimensional (2D) material with unique electrical and chemical properties [1]. These include extremely high Young's modulus and fracture stress [2], high electrical conductivity [3, 4], excellent thermal conductivity [5], low contact resistance [6], high mobility [7], large specific surface area, and high light transmittance and flexibility [8]. Therefore, graphene can be developed and applied in various fields [9], such as high-quality composite materials [10], biomedical and drug delivery [11], transistors [12, 13], integrated circuits [14], flexible electronics [15] and energy storage devices [16].

Owing to the excellent properties of 2D graphene [17], its three-dimensional (3D) counterpart is widely used in gas molecular sensors owing to its unique 3D nanoporous structure [18], and feasible surface functionalization [19]. The resistance of the graphene-based chemiresistor [20] changes with the introduction of gases, which is the gas-sensing mechanism.

Compared with other carbon nanomaterials [21], graphene has the advantages of high conductivity and a large, theoretical, specific surface area (3523 $m^2\ g^{-1}$) [22]. These facilitate the effective adsorption of gas molecules. Graphene shows excellent prospects for gas-sensing applications [23]. Three-dimensional graphene interacts with different compositions and structures of gas adsorbents [24] in diverse ways. The gaseous molecule adsorbs onto graphene by weak Van der Waals interactions; hence, the resistance of graphene can be monitored by uncomplicated electrical equipment [25]. Owing to its high-quality lattice structure [26], 3D graphene possesses inherently low electrical noise, which avoids large charge fluctuations compared with carbon nanotubes [27]. In addition, chemiresistor-based sensing formats possess the advantages of simple equipment, easy fabrication, and direct measurement [28].

With the improvement in human living standards and increasing attention to environmental protection, air quality, and atmospheric pollution, more significant requirements for gas monitoring have been introduced [29]. Air pollution indoors and inside vehicles threatens human health and has become a common concern worldwide. Among the existing hazardous gases, formaldehyde is a common representative example [30]. It is a colorless and soluble irritant gas, which is volatile in adhesive decoration materials such as wallpaper. High concentrations of 20 to 100 ppm are detrimental to health and well-being [31, 32], while long-term exposure to lower levels can cause allergies, carcinogenesis, and mutations [33, 34]. Among all contacts, children (leukemia rate) and pregnant women (abortion rate) are particularly sensitive.

Therefore, an effective formaldehyde gas sensor is an immediate safety requirement. Among the existing formaldehyde sensors, some of them rely on amperometric techniques, requiring either UV irradiation [35] or enzymes [36] as receptors, which are prone to conformational changes and, therefore, show poor long-term stability or require special storage conditions.

Indeed, conventional semiconductor sensor requires high operation temperature [37–39] or external UV-light activation [35]. The graphene has the advantage of high conductivity at low operation temperature, which often was blended with semiconducting oxides for improving the surface area and conductivity. Indeed, graphene/metal oxides based composites could improve the sensitivity of formaldehyde sensor because of the electron transfer channels provided by the metal oxide such as SnO [40], SnO_2 [39, 41, 42], TiO_2 [43–45], and ZnO [46–48] and $ZnSnO_3$ [49]. Besides, the graphene has formed composites with polymers [50–52], Si nanowires [53] and MoS_2 [54, 55] to serve as formaldehyde-sensing materials. However, the oxygen plasma treated 3D graphene has yet applied in formaldehyde sensing.

Therefore, we employed 3D graphene with different treatments and compared their structure-performance relationships. In this study, we applied three strategies to treat 3D graphene, including untreated, HNO_3 etching, and oxygen plasma treatment and their application in chemiresistors for gas sensing using formaldehyde as an example.

Experimental details

Synthesis of 3D graphene by chemical vapor deposition (CVD)

The Ni foam was washed with HCl (19 vol%), then washed with deionized water. The pre-treated Ni foam was placed in a quartz boat and deposited in the center of the furnace (figure S1 (available online at stacks.iop.org/NANO/33/185702/mmedia)). First, the tubular furnace was vacuum pumped to 10 Pa to remove air and water. Second, the fixed carrier gas rate was 270/30 ml min^{-1} Ar/H_2 after high-speed cleaning with a large flow of Ar/H_2 to atmospheric pressure. It was heated at 70 °C min^{-1} and annealed at 1028 °C for 15 min. Further, 20 sccm CH_4 as growth gas was injected for 1 h, then rapidly cooled to room temperature.

Freestanding 3D graphene without Ni

First, 3D graphene fabricated by CVD was soaked in 2M $FeCl_3$ mixed solution to remove the Ni substrate. The fully etched 3D graphene was then transferred to deionized water (mixed with HCl acid) for 2 h. Here, the HCl solution was diluted to 0.37 wt% with deionized water. Then, the soaking in diluted HCl was repeated for three times for thoroughly removing the residual Fe species. Indeed, the titer by the transfer recipe has been well established in our group for thorough removal of Fe removal, i.e. no emergence of Fe atoms over graphene in TEM images [17, 56], which have been commonly observed by the Cs-corrected atomic resolution TEM imaging [57, 58]. Eventually, the freestanding 3D graphene was dried naturally at 25 °C for storage, characterizations, and device fabrications.

Posttreatment of 3D graphene

Three approaches were employed for graphene posttreatment (Table S1). First, non-treatment was conducted on the 3D graphene. The second treatment was the HNO_3 etching of 3D graphene. The synthesized 3D graphene was submerged in HNO_3 (34 wt%) for 24 h. Third, the 3D graphene was treated with oxygen plasma (Diener Electronic, model: Atto-BLS). Initially, the chamber was vacuumed at 20 Pa. Then, oxygen at a flow rate of 10 ml min^{-1} was introduced into the chamber. Further, the oxygen plasma was generated at an RF power (13.56 MHz) of 90 W and treated for 5–30 min. The plasma-induced defects in 3D graphene were characterized using Raman spectroscopy. Eventually, 15 min was found to be optimal for completely functionalizing graphene with oxygen.

Material characterization

Optical microscopy (Olympus BX53MRF-S) was used to obtain snapshot optical micrographs. Raman spectra and mapping were performed using 532 nm excitation wavelength Raman spectroscopy (Horiba Labram HR800). The present chemical bonds or functional groups were determined using a Fourier transform infrared spectrometer (Bruker VERTEX 70 FT-IR). The phase structure was tested using x-ray diffractometry (Thermo Fisher ARL Equlnox 3000). The surface morphologies were investigated using a scanning electron microscope (Hitachi Regulus8100). The lattice structure, selected area electron diffraction, and elemental analysis were conducted using a transmission electron microscope (JEOL JEM-2100) integrated with energy-dispersive x-ray spectroscopy.

Device fabrication

Three types of post-treated 3D graphene (2 × 2 cm^2) were transferred to glass slides with patterned Au electrodes (50 nm Au). Gold electrodes were fabricated on glass slides using an electron-beam evaporator (HHV ATS 500). The 3D graphene was aligned and adhered to bridge to two adjacent Au electrodes (figure S9).

Gas-sensing examination

A simple gas chamber was used to test for the presence or absence of resistive 3D graphene based sensors. A 25 ml formaldehyde solution (Sigma-Aldrich, 38%) was dropped onto a hot plate (30 °C) to generate formaldehyde vapor. The relative humidity was maintained at 30%, and the temperature was maintained at 25 °C.

The concentration of the targeted gas molecule was measured from the mean of the static liquid distribution, which was calculated using the following equation:

$$C = \frac{22.4 \times \Phi \times \rho \times V_1}{M \times V_2} \times 1000 \text{ ppm},$$

where C (ppm) is the concentration of the target gas, Φ is the volume fraction of the target gas molecule, ρ (g ml^{-1}) is the density of the liquid, V_1 (ml) is the volume of the test liquid, V_2 (l) is the volume of the test chamber, and M (g mol^{-1}) is the molecular weight of the test liquid.

The time-dependent current curves of the gas sensor were collected using a source measurement unit (Keithley 2400). The response and recovery times were determined from the time-dependent current curves of the gas sensors. The response time of the sensor was determined when the resistance (in gas) dropped to 90% of the pristine resistance (in air) during the adsorption process. The recovery time was determined when the resistance dropped to 90% upon the desorption of gas molecules.

Results and discussion

Three different treatments of 3D graphene after growth were investigated and compared in this study. These labels are provided in Table S1, and each experiment in the text and graphics employs the same label. The 3D graphene treatments were non-treatment, oxygen plasma, and etching in HNO_3 solution.

We first discuss the appearance and morphology of the 3D graphene observed by optical microscopy (figure 1) to confirm the homogeneity of the large area of the synthesized 3D graphene.

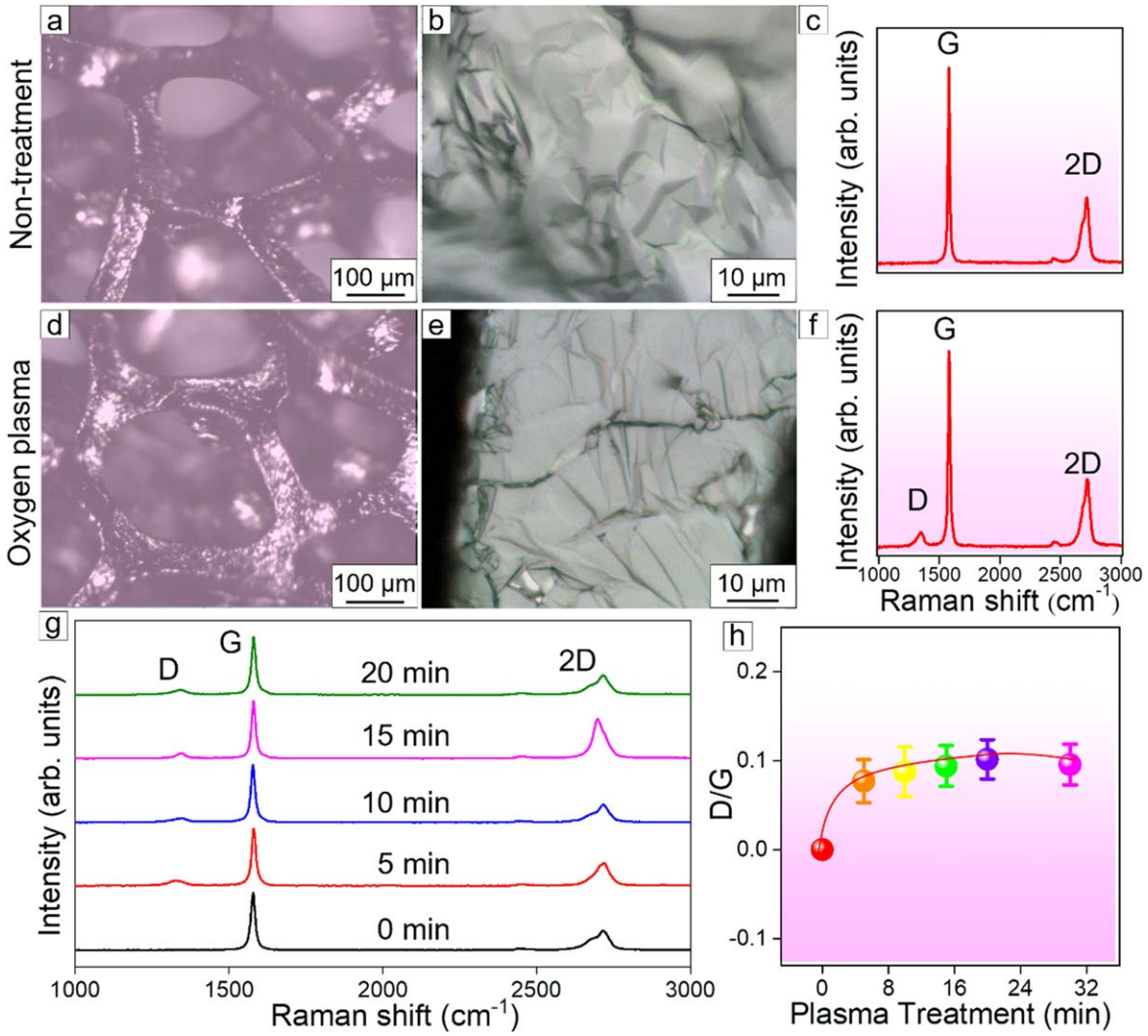

Figure 1. Morphology and Raman spectra of 3D graphene with and without oxygen plasma treatment. (a), (b) The optical microscopic images of non-treated 3D graphene (over Ni foam) with different magnifications. (c) The Raman spectrum of non-treated 3D graphene. The peak positions were assigned for D mode (ca. 1350 cm^{-1}), G mode (ca. 1580 cm^{-1}) and 2D mode (ca. 2700 cm^{-1}). (d), (e) The optical microscopic graphs and (f) Raman spectrum of 3D graphene after treatment with oxygen plasma. The Raman spectra and D/G ratio of oxygen plasma-treated 3D graphene. (g) The Raman spectra of oxygen plasma-treated 3D graphene for different durations of (from bottom to top) 0, 5, 10, 15, 20 min. (h) Statistics of the D/G ratio of the oxygen plasma-treated 3D graphene after different treatment times.

The 3D graphene synthesized by CVD had a large 3D framework structure (figure 1(a)) and high surface uniformity (figure 1(b)). The 3D graphene treated by oxygen plasma maintained the intrinsic 3D framework property (figure 1(d)) and homogeneous surface uniformity (figure 1(e)). This illustrated that the posttreatment of oxygen plasma did not affect the morphology of 3D graphene. Besides, the HNO_3 treatment has caused negligible changes in morphology and structure of 3D graphene (figure S6).

Raman spectroscopy is a powerful tool for exploring the properties of graphene. The quality and purity of the synthesized 3D graphene was determined by Raman spectroscopy. It was also used to analyze the number of layers of the grown graphene films on the substrate of the Ni foam. The Raman spectrum illustrated the monolayer property through peaks at ca. 1580 cm^{-1} for the G mode and ca. 2700 cm^{-1} for the 2D mode (figure 1(c)). The emergence of the D mode (ca. 1350 cm^{-1}) indicated graphene defects (figure 1(f)). Hence, 3D graphene treated by oxygen plasma may lead to defects due to surface functionalization.

After the posttreatment with oxygen plasma, 3D graphene possessed oxygen-containing groups. For example, carbonyl and epoxy groups, this is further discussed with the infrared spectra. These structural defects were determined by Raman spectroscopy. The Raman spectra of 3D graphene with different oxygen plasma treatment times are shown in figure 1(g). Oxygen functionalization often occurred at the surface and the edges of the 3D graphene [59] upon the introduction of plasma. Specifically, no oxygen was incorporated into the interlayer spacing of few-layer graphene [60]. Therefore, surface oxygen functionalization could achieve a saturable condition on the graphene surfaces. We used the D/G ratio in the oxygen-plasma-treated graphene to determine the saturation of oxygen functionalization. Oxygen

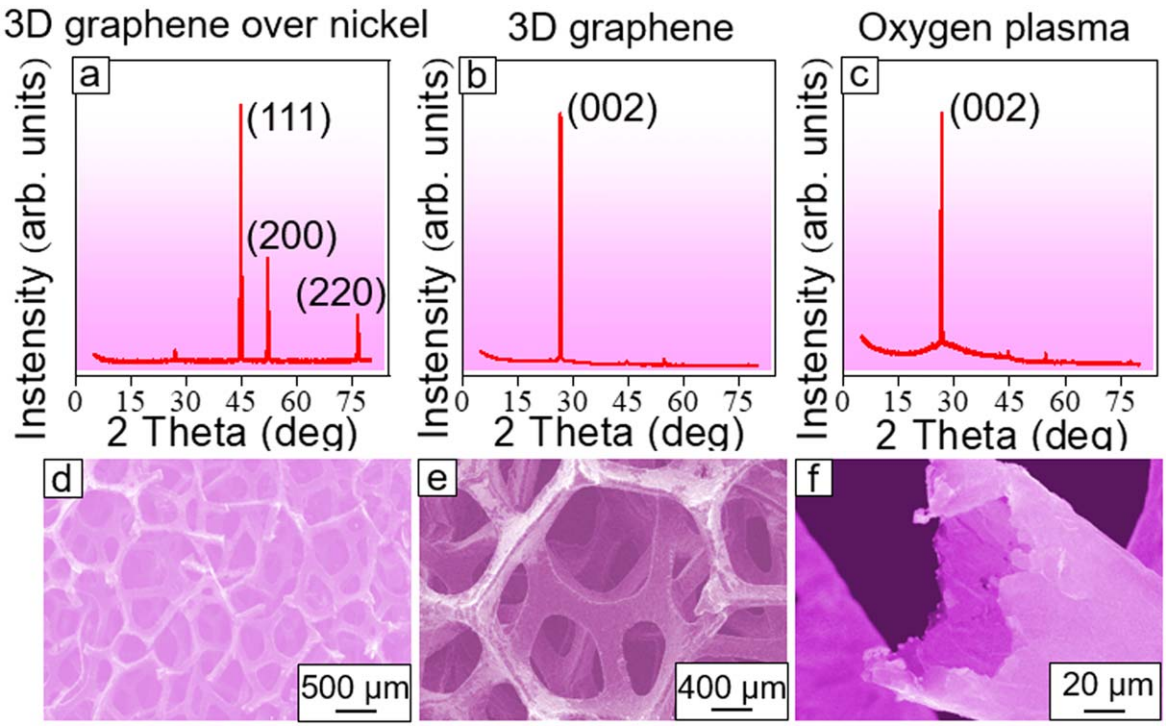

Figure 2. Diffraction spectra and surface morphology of 3D graphene. (a) The x-ray diffraction (XRD) spectrum of the 3D graphene supported by Ni foam. The XRD spectra of (b) 3D graphene (after Ni removal) and (c) 3D graphene (after Ni etching) treated by oxygen plasma. (d)–(f) SEM micrographs for oxygen treated 3D graphene (after Ni removal). In panel (f), a hollow tube of 3D graphene was presented.

saturation occurred when the D/G ratio ceased to increase with prolonged plasma treatment. After 15 min of oxygen plasma the D/G ratio (0.10) of graphene stabilized (figure 1(h)).

Pristine 3D graphene does not show D mode in Raman spectrum (figure 1(c)). With 5 min oxygen plasma treatment, the graphene exhibits significant D mode (figure 1(g)). After extending the oxygen plasma duration from 5 min to 20 min, the D/G intensity ratio increases to 0.1 (figure 1(h)). Further oxygen plasma treatment, i.e. for 30 min, does not induce larger D/G ratio. Therefore, we selected an oxygen plasma duration of 15 min for the graphene treatment and subsequent device fabrication.

To show the crystal quality, we compared pure 3D graphene and Ni-supported 3D graphene by x-ray diffraction (figure 2).

The purity of the 3D graphene was analyzed after etching. The 3D graphene supported by the Ni framework (figure 2(a)) showed an obvious face-centered cubic peak of Ni metal at ca. $2\theta = 44.4^\circ$ (111), ca. $2\theta = 51.7^\circ$ (200), and ca. $2\theta = 76.3^\circ$ (220), respectively. The XRD graph of the pure 3D graphene (figure 2(b)) after etching exhibits one peak (002). This confirmed the success of etching as no Ni residue or other impurities remained.

The XRD pattern of the synthesized 3D graphene showed a diffraction peak at $2\theta = 26.6^\circ$ (figure 2(b)). The estimated layer spacing of graphene was 0.335 nm by the Bragg equation $2d\sin\,\theta = n\lambda$, which was the result of the preferred orientation of the graphene reflection. A noticeable reflection of the (002) peak demonstrated that the grown 3D graphene was arranged regularly along the stacking direction.

Compared with the non-treatment of 3D graphene, the 3D graphene after oxygen plasma treatment (figure 2(c)) showed the same single strength peak at the crystal plane of (002), which indicated that the posttreatment of oxygen plasma did not destroy the initial crystal structure. In addition, we did not see the emergence of the GO peak at around 10 degrees [61]. Again, the oxygen-plasma treatment does not change the crystal structure of graphene, i.e. without the formation of graphene oxide. In addition, the HNO_3 treatment did not cause change in crystal structure of graphene (figure S8) as XRD data show.

To further study the surface morphology characteristics of 3D graphene, scanning electron microscopy (SEM) was used for more detailed observation and characterization. After etching the Ni framework, 3D graphene retained the interconnected 3D supporting structure of the original Ni foam template (figure 2(d)) and a large hollow tube (figure 2(f)). The pore size of the 3D graphene was mainly distributed in the range of 300–500 μm (figure 2(e)), which was consistent with the diameter of the hole of the Ni foam. Therefore, the synthesized 3D graphene possessed structural integrity and size stability.

The crystal structure and characteristics of the synthesized 3D graphene after treatment with oxygen plasma were analyzed through imaging and electron diffraction of the transferred 3D graphene (figure 3).

The low-magnification TEM graph (figure 3(a)) demonstrated the smooth homogeneity of the surface of the 3D

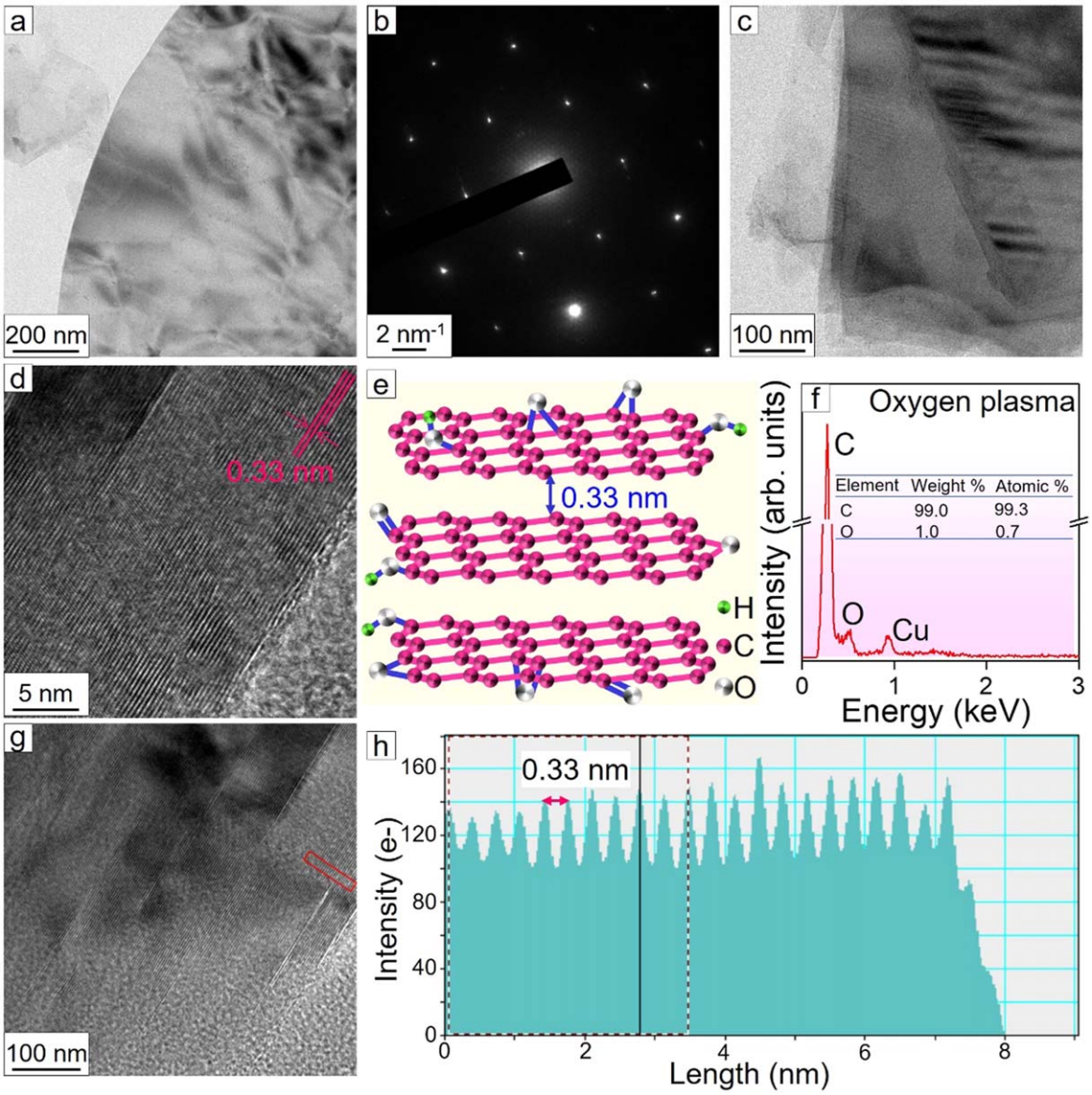

Figure 3. Structural, elemental, and diffraction analysis of the oxygen-plasma-treated 3D graphene. (a) Low-magnification transmission electron microscope graph of graphene (transferred) over a Quantifoil grid. (b) Selected area electron diffraction (SAED) pattern of the graphene. (c) TEM micrograph of graphene with fringes and (d) high-magnification TEM micrographs showing the layer stacks of the graphene. (e) The surface atomic diagram of the multilayer graphene. (f) Energy-dispersive x-ray spectrum of the oxygen plasma-treated 3D graphene. (g) TEM graph showing the stacked layers of few-layer 3D graphene. (h) The intensity profile of the interlayer spacing of graphene in panel (g).

graphene after treatment with oxygen plasma. The SAED (figure 3(b)) exhibited a [100] lattice plane with six-fold symmetry of the 3D graphene crystal. The TEM micrograph of graphene with fringes (figure 3(c)) showed the 3D graphene layers (ca. 8–10), which was illustrated by the micro-nano-crystalline surface (figure 3(d)). The surface atomic diagram of the multilayer graphene demonstrated the distribution of the epoxy and carbonyl groups (figure 3(e)). The TEM data show negligible difference for pristine 3D graphene (figure S2) and HNO_3 treated 3D graphene (figure S3), compared to the oxygen plasma treated sample.

Now we come to discuss the defects and the oxygen contents of graphene by three types of treatments. CVD-grown graphene over Ni foam was free of defects, i.e. none D mode in Raman spectrum. The oxygen plasma seems to introduce sp^3 type defects, e.g. hydroxyl or epoxy groups in our experiments (figure 3(e)). Indeed, the vibrational modes and chemical environments of these oxygen-related bonds were confirmed later as FT-IR (figure 4) and XPS data (figures S4 and S5) indicate. The structure disorder in graphene, often termed defects, e.g. sp^3 type, could be induced with plasma treatments [62, 63]. Indeed, the plasma could introduce defects both at edges and on the basal planes as tip-enhanced Raman spectroscopy mapping shows [64]. Besides, vacancy-type defects were often observed with heavily ions-irradiated graphene surfaces [65–68]. The graphene edges contribute to the D modes under Raman spectroscopic characterizations [69–71].

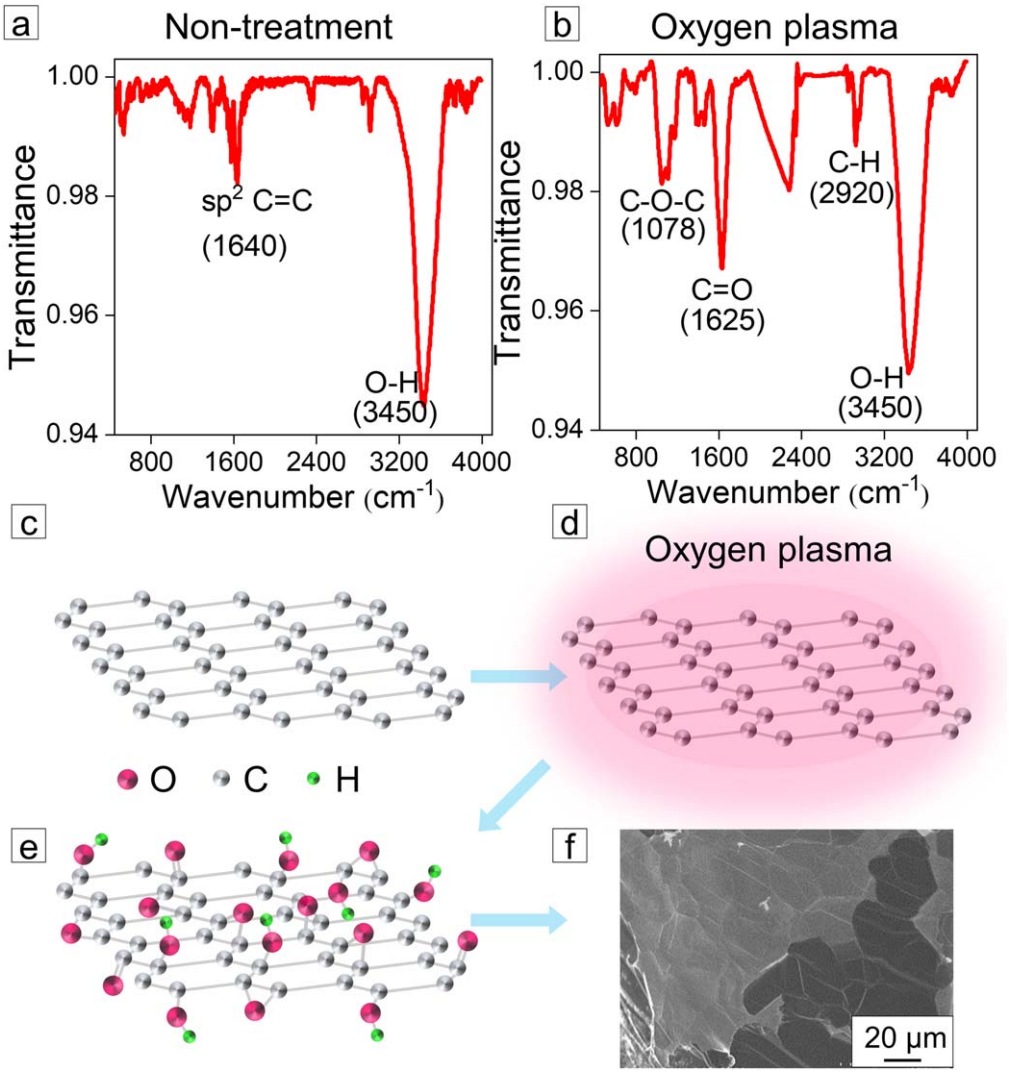

Figure 4. Infrared spectra of 3D graphene without (a) and with (b) oxygen plasma treatment. Oxygen plasma leads to the formation of epoxy groups and carbonyl radicals at the edges and on the surface of graphene. The atomic configuration of graphene during plasma treatment (c) pristine graphene, (d) initial oxygen plasma, and (e) complete plasma treatment. The oxygen-containing groups are distributed over the surface of graphene, such as the carbonyl, aldehyde, and epoxy groups. (f) A typical SEM micrograph of the oxygen plasma-treated 3D graphene.

The pristine 3D graphene contains the minimum oxygen content (0.4 at%) as EDX data show (figure S2(e)), which corresponding to hydroxyl group (figure 4(a)). Then, the 3D graphene treated by oxygen plasma is less (figure 3(f)), i.e. 0.7 at%, corresponding to the hydroxyl groups as indicated by infrared spectra (figure 4(b)). In addition, the oxygen content of three-dimensional graphene etched by nitric acid is the highest (0.8 at%), (figure S3(e)) which corresponds to the enhancement of C–O group in the peak shown by infrared transmittance spectrum (figure S7(a)). The hydroxyl groups are preferred for the rapid response to formaldehyde gas molecules compared to other oxygen-containing groups (discussed later in the section of sensing mechanism).

The TEM graph exhibited typical graphitic fringes along smooth edges, which indicated multilayer graphene features (figure 3(g)). The measurement of the interlayer spacing of the 3D graphene was ca. 0.33 nm (figure 3(h)).

We compared the infrared spectra of the 3D graphene with and without oxygen plasma. The strong absorption peak of O–H was at ca. 3450 cm^{-1} (figure 4(a)). This was caused by the hydrogen bond adhering to the graphene surface during the plasma etching. This was caused by the hydrogen bond adhering to the graphene surface during the plasma etching [59, 72].

Compared to the non-treated 3D graphene, the post-treatment with oxygen plasma sample showed an absorption peak at ca. 2700 cm^{-1} (−CHO), and a stronger stretching vibration peak of C=O at 1625 cm^{-1} (figure 4(b)) [73]. In addition, the absorption peaks emerge at ca. 2900 cm^{-1} (including two peaks at 2920 and 2850 cm^{-1}), which are assigned as the C–H stretching modes [74, 75]. Therefore, oxygen-containing functional groups were introduced across the surface of 3D graphene (figure 4(e)). These oxygen-containing groups were more likely to adsorb formaldehyde gas

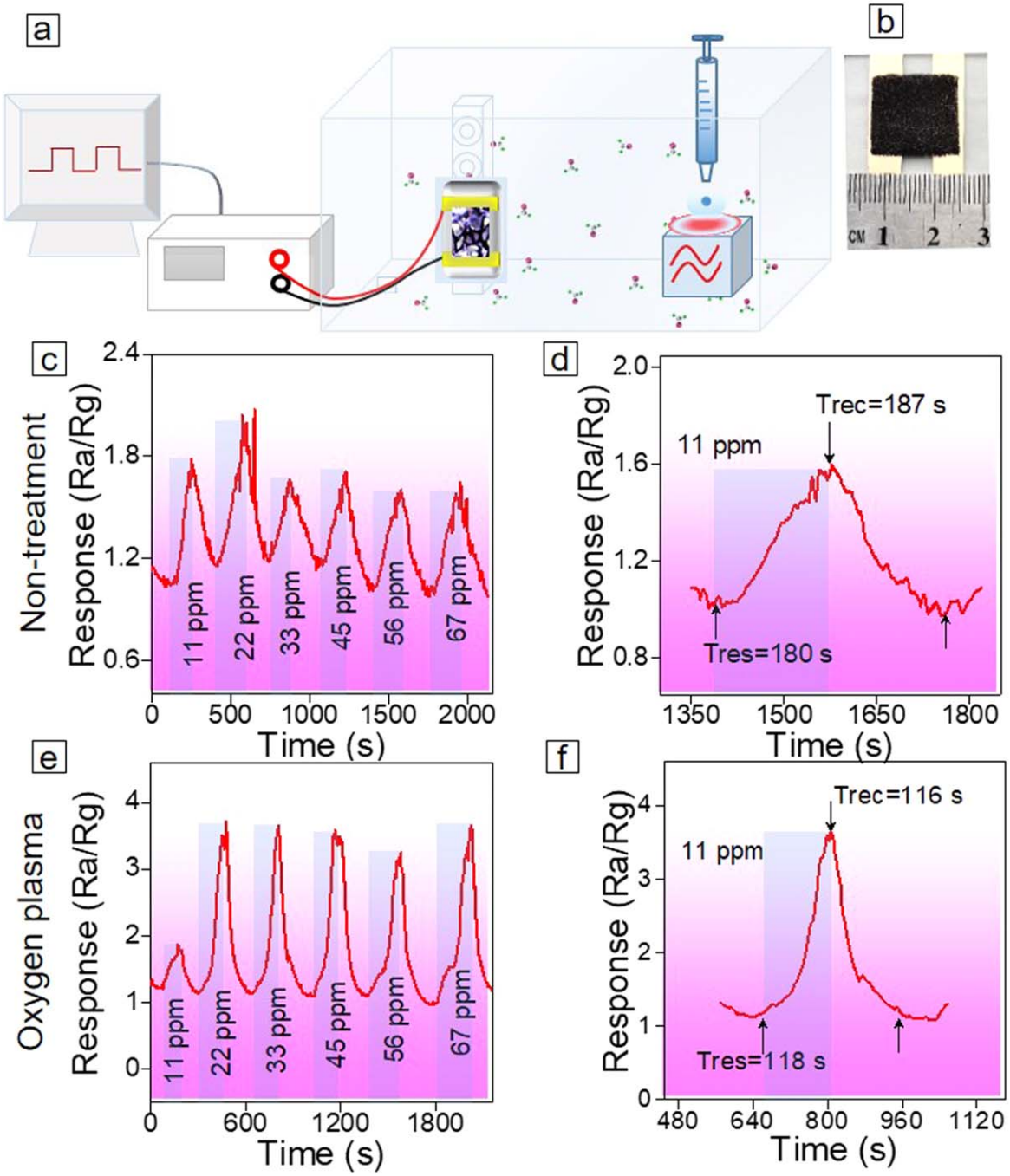

Figure 5. Gas-sensing performances of 3D graphene with and without oxygen plasma treatment. (a) The gas sensor testing platform schematic includes a test chamber, electric measurement equipment (source measurement unit), and a gas introducing unit. (b) The photograph of the gas sensor based on the oxygen plasma-treated 3D graphene bridging two Au electrodes. (c), (d) Response curve of the gas sensor based on the untreated 3D graphene. The response is the quotient of the Ra/Rg. Ra denotes the resistance of 3D graphene in open air. Rg denotes the resistance of 3D graphene with introducing the target gas. (e), (f) The response performances of the gas sensor based on oxygen plasma-treated 3D graphene. Different concentrations of formaldehyde molecules were introduced during the sensor examination.

molecules, which was consistent with the performance tests for the detection of formaldehyde molecules (discussed later).

We examined the gas-sensing performance of the three types of post-treated 3D graphene. The electric current of the sensor was tested at a fixed voltage (0.1 V). Liquid formaldehyde was injected and dropped onto a hot plate (30 °C) (figure S10). At high temperatures, formaldehyde volatilized into gaseous molecules, which filled the gas test chamber (figure 5). A large specific surface area and high quality of 3D graphene have been demonstrated in the detection of gas molecules. The analysis of response and recovery confirmed the gas sensitivity of the 3D graphene-based gas sensor at a formaldehyde concentration of 11 ppm at 25 °C.

The untreated 3D graphene exhibited a stable response and excellent repeatability for exposure to a formaldehyde concentration of 11 ppm. This demonstrated that the sensor

had significant detection ability at lower concentrations of gas molecules (figure 5(c)). The HNO_3-treated 3D graphene showed weak performance during gas sensing. The devices had poor recovery upon ventilation (figure S12).

Comparatively, the oxygen plasma-treated sample (figure 5(e)) showed a shorter response time (ca. 118 s versus 180 s for the untreated 3D graphene) and faster recovery time (ca. 116 s versus 187 s for the untreated 3D graphene) (figures 5(d) and (f)). Our device performances were comparable to the best devices ever reported with some oxide assistance (table S2).

The detection mechanism was determined by analyzing the response current curves. First, the three types of treatments do not significantly change their conductance (figure S11). This means the good electric transport has been maintained for graphene. And the oxygen functionalization only occurs at the topmost layer surface or edges of the graphene (ca. 10 layers as HRTEM data show). Then, the gas interaction occurs at the surface of graphene, other than the interlayers. Here, the electron-rich formaldehyde molecule as a donor was adsorbed onto the surface of 3D graphene, which increased the electron cloud density of 3D graphene and the number of carriers. Therefore, 3D graphene absorbed the gas molecules of formaldehyde, which improved the measured conductivity.

Now we come to discuss the chemistry behind the enhanced gas sensing capability after oxygen plasma treatment. The hydroxyl was found to account for the sensing of oxygen-containing polar molecules. As per ab initio calculation, the hydroxyl exhibits the highest affinity to formaldehyde molecules than that of the epoxy and carbonyl [76]. Besides, the hydroxyl can form the hydrogen bonds with oxygen from formaldehyde, which lead to a stable gas/hydroxyl interaction [77]. And the rotational deformation of hydroxyl [78] facilitates the acquisition of gaseous molecules upon the adsorption. Eventually, a drastic charge transfer occurs between gaseous molecules and the graphene, viz., a change emerges in the conductance of graphene based chemiresistor. For example, the electrons transfer from the nitrogen at ammonia to hydroxyl at graphene [77]. In comparison, the electrons are extracted from HCHO to reduced graphene oxides [48, 54, 79, 80]. However, the pristine graphene acts as electron acceptor when interacting with formaldehyde [81]. Indeed, the carbon-containing groups can regulate the electric property of graphene by the sp^3 hybridization [82, 83], which leads to the decrease of delocalized π electrons [84]. Therefore, the variation of graphene conductance [85, 86] leads to the sensitivity of gas detection through the rapid change of conductance [87, 88]. However, these oxygen elements are of low percentage compared to carbon, which do not change much the metallic conductivity of graphene [89, 90], i.e. without doping. This maintains the good response upon the introduction of gas molecules [91]. Upon the release of gas molecules, the structure of hydroxyl turns back to its initial state, which features fast recovery of gas sensors.

However, the oxygen of epoxy group has lone-pair electrons which could expel the rich electrons at the formaldehyde [92]. Therefore, epoxy is not preferred in the gas sensing of electron-rich oxygen at HCHO molecules [93–95]. And the HNO_3 treatment leads to the epoxy functionalization of graphene [96].

Compared with graphene oxides, our 3D graphene foam after oxygen plasma treatment retains good electric conductivity, which allows good rise/recovery rate. Besides, our 3D graphene-based sensor could operate at room temperature. Indeed, the extraordinary performances of oxygen treated 3D graphene-based gas sensors result in the mild oxidation that occurs dominantly at the surface. Therefore, the surface functionalization facilities the interaction of gas molecules. Meanwhile the good electric conductivity guarantees the fast charge transfer, which leads to extraordinary response. The hydroxyl group are dominant for the capture and release of gas molecules, which retains the excellent long-term cycling performances of the devices.

Our experimental results of sensing HCHO confirm high performances of oxygen plasma treated graphene due to hydroxyl-rich surface functionalization; and low performance of HNO_3 treated graphene (figure S12) by epoxy-rich groups. Indeed, the oxygen plasma treatment led to the formation of hydroxyl at graphene surfaces while the HNO_3 treatment leads to the epoxy introduction over graphene. Our results show the superior performances of oxygen plasma treated graphene for formaldehyde detection. This may provide a guide rule for the functionalization of other 2D materials and their sensor applications.

Conclusions

We prepared oxygen plasma-treated 3D graphene for chemiresistor fabrication and demonstrated the high gas-sensing performance with formaldehyde as an example. Compared with non-treatment and HNO_3 etching, oxygen plasma treatment showed a superior approach for the functionalization of graphene with the epoxy group and carbonyl radicals. The structural functionalization was reflected in the excellent gas-sensing performance based on oxygen plasma-treated 3D graphene. The response time was shortened by 34%, and the recovery time was decreased by 38% compared to pristine 3D graphene. In addition, treatment with the oxygen plasma for 15 min resulted in the best gas-sensing performance. Our findings may boost research progress in chemiresistor-based gas sensing.

Acknowledgments

The authors are grateful to the Natural Science Foundation of Shandong Province, China (Grant No. ZR2019BEM040) and the National Natural Science Foundation of China (NSFC grant No. 51802116). The authors acknowledge the financial support of the Project of '20 items of University' of Jinan (2018GXRC031). WZ thanks NSFC (Grant No. 52022037) and Taishan Scholars Project Special Funds (TSQN201812083). This work was financially supported by Key Research and

Development Program of Shandong Province (grant No. 2020CXGC010602), Science and Technology Support Plan for Young People in Colleges and Universities of Shandong Province (grant No. 2020KJE005). The Project was supported by the Foundation (No. GZKF202107) of State Key Laboratory of Biobased Material and Green Papermaking, Qilu University of Technology, Shandong Academy of Sciences. MHR thanks the National Science Foundation China (NSFC, Project 52071225), the National Science Center, and the Czech Republic under the European Regional Development Fund (ERDF) program 'Institute of Environmental Technology-Excellent Research' (Grant No. CZ.02.1.01/0.0/0.0/16_019/0000853), and the Sino-German Research Institute for Support (Project No. GZ 1400).

Data availability statement

The data generated and/or analysed during the current study are not publicly available for legal/ethical reasons but are available from the corresponding author on reasonable request.

ORCID iDs

Jinbo Pang https://orcid.org/0000-0001-6965-4166

References

[1] Kovalev S *et al* 2021 Electrical tunability of terahertz nonlinearity in graphene *Sci. Adv.* **7** eabf9809
[2] Cui T, Mukherjee S, Sudeep P M, Colas G, Najafi F, Tam J, Ajayan P M, Singh C V, Sun Y and Filleter T 2020 Fatigue of graphene *Nat. Mater.* **19** 405–11
[3] Aharon-Steinberg A, Marguerite A, Perello D J, Bagani K, Holder T, Myasoedov Y, Levitov L S, Geim A K and Zeldov E 2021 Long-range nontopological edge currents in charge-neutral graphene *Nature* **593** 528–34
[4] Epstein I *et al* 2020 Far-field excitation of single graphene plasmon cavities with ultracompressed mode volumes *Science* **368** 1219–23
[5] Huang Y, Tao L-Q, Yu J, Zheng K, Wang G and Chen X 2020 Improved performance of flexible graphene heater based on repeated laser writing *IEEE Electron Device Lett.* **41** 501–4
[6] Dipalo M *et al* 2021 Intracellular action potential recordings from cardiomyocytes by ultrafast pulsed laser irradiation of fuzzy graphene microelectrodes *Sci. Adv.* **7** eabd5175
[7] Niu W *et al* 2020 A curved graphene nanoribbon with multi-edge structure and high intrinsic charge carrier mobility *J. Am. Chem. Soc.* **142** 18293–8
[8] Sun B J *et al* 2021 Synthesis of wafer-scale graphene with chemical vapor deposition for electronic device applications *Adv. Mater. Technol.* **6** 2000744
[9] Yuan Z, Li J, Yang M, Fang Z, Jian J, Yu D, Chen X and Dai L 2019 Ultrathin black phosphorus-on-nitrogen doped graphene for efficient overall water splitting: dual modulation roles of directional interfacial charge transfer *J. Am. Chem. Soc.* **141** 4972–9
[10] Arndt C *et al* 2021 Microengineered Hollow graphene tube systems generate conductive hydrogels with extremely low filler concentration *Nano Lett.* **21** 3690–7
[11] Kim M, Porras-Gomez M and Leal C 2020 Graphene-based sensing of oxygen transport through pulmonary membranes *Nat. Commun.* **11** 1103
[12] Tao L, Chen Z, Li Z, Wang J, Xu X and Xu J B 2020 Enhancing light-matter interaction in 2D materials by optical micro/nano architectures for high-performance optoelectronic devices *InfoMat* **3** 36–60
[13] Kaidarova A and Kosel J 2021 Physical sensors based on laser-induced graphene: a review *IEEE Sens. J.* **21** 12426–43
[14] Jiantao Ping L Q, Quanbo W, Shuhua L, Jiang Y, Li Y, Lin J-M and Hua Q 2021 An integrated liquid crystal sensing device assisted by the surfactant-embedded smart hydrogel *Biosens. Bioelectron.* **187** 113313
[15] Shi Q, Dong B, He T, Sun Z, Zhu J, Zhang Z and Lee C 2020 Progress in wearable electronics/photonics-Moving toward the era of artificial intelligence and internet of things *InfoMat* **2** 1131–62
[16] Jayaramulu K *et al* 2021 Covalent graphene-MOF hybrids for high-performance asymmetric supercapacitors *Adv. Mater.* **33** 2004560
[17] Pang J, Bachmatiuk A, Fu L, Yan C, Zeng M, Wang J, Trzebicka B, Gemming T, Eckert J and Rummeli M H 2015 Oxidation as a means to remove surface contaminants on cu foil prior to graphene growth by chemical vapor deposition *J. Mater. Chem. C* **119** 13363–8
[18] Roslon I E *et al* 2020 High-frequency gas effusion through nanopores in suspended graphene *Nat. Commun.* **11** 6025
[19] An N *et al* 2020 Electrically tunable four-wave-mixing in graphene heterogeneous fiber for individual gas molecule detection *Nano Lett.* **20** 6473–80
[20] Tiwari J N, Vij V, Kemp K C and Kim K S 2016 Engineered carbon-nanomaterial-based electrochemical sensors for biomolecules *ACS Nano* **10** 46–80
[21] Das C M, Kang L, Ouyang Q and Yong K T 2020 Advanced low-dimensional carbon materials for flexible devices *InfoMat* **2** 698–714
[22] Zhang L *et al* 2013 Porous 3D graphene-based bulk materials with exceptional high surface area and excellent conductivity for supercapacitors *Sci. Rep.* **3** 1408–12
[23] Huang S, Panes-Ruiz L A, Croy A, Löffler M, Khavrus V, Bezugly V and Cuniberti G 2021 Highly sensitive room temperature ammonia gas sensor using pristine graphene: The role of biocompatible stabilizer *Carbon* **173** 262–70
[24] Pang J *et al* 2015 Direct synthesis of graphene from adsorbed organic solvent molecules over copper *RSC Adv.* **5** 60884–91
[25] Pang J, Bachmatiuk A, Ibrahim I, Fu L, Placha D, Martynkova G S, Trzebicka B, Gemming T, Eckert J and Rümmeli M H 2015 CVD growth of 1D and 2D sp^2 carbon nanomaterials *J. Mater. Sci.* **51** 640–67
[26] Pang J *et al* 2017 Self-terminating confinement approach for large-area uniform monolayer graphene directly over Si/SiO_x by chemical vapor deposition *ACS Nano* **11** 1946–56
[27] Wang M *et al* 2020 Phthalocyanine-based 2D conjugated metal-organic framework nanosheets for high-performance micro-supercapacitors *Adv. Funct. Mater.* **30** 2002664
[28] Akhter F, Alahi M E E, Siddiquei H R, Gooneratne C P and Mukhopadhyay S C 2021 Graphene oxide (GO) coated impedimetric gas sensor for selective detection of carbon dioxide (CO_2) with temperature and humidity compensation *IEEE Sens. J.* **21** 4241–9
[29] Cheng Q *et al* 2020 WSe_2 2D p-type semiconductor-based electronic devices for information technology: design, preparation, and applications *InfoMat* **2** 656–97

[30] Li B *et al* 2019 An investigation of formaldehyde concentration in residences and the development of a model for the prediction of its emission rates *Build. Sci.* **147** 540–50

[31] OSHA 2011 *Fact Sheet: Formaldehyde* (Washington: Occupational Safety and Health Administration, United States Department Of Labor)

[32] Health N J 2016 The right to know hazardous substance fact sheet *Formaldehyde* (Trenton: New Jersey Department of Health)

[33] Golden R 2011 Identifying an indoor air exposure limit for formaldehyde considering both irritation and cancer hazards *Crit. Rev. Toxicol.* **41** 672–721

[34] Kaden D A, Mandin C, Nielsen G D and Wolkoff P 2010 *WHO Guidelines for Indoor Air Quality: Selected Pollutants* (Geneva: WHO Regional Office for Europe)

[35] Peng L, Zhao Q, Wang D, Zhai J, Wang P, Pang S and Xie T 2009 Ultraviolet-assisted gas sensing: A potential formaldehyde detection approach at room temperature based on zinc oxide nanorods *Sensors Actuators B* **136** 80–5

[36] Achmann S, Hermann M, Hilbrig F, Jerome V, Hammerle M, Freitag R and Moos R 2008 Direct detection of formaldehyde in air by a novel NAD^+- and glutathione-independent formaldehyde dehydrogenase-based biosensor *Talanta* **75** 786–91

[37] Chu X, Chen T, Zhang W, Zheng B and Shui H 2009 Investigation on formaldehyde gas sensor with ZnO thick film prepared through microwave heating method *Sensors Actuators B* **142** 49–54

[38] Gao X, Li F, Wang R and Zhang T 2018 A formaldehyde sensor: significant role of p-n heterojunction in gas-sensitive core-shell nanofibers *Sensors Actuators B* **258** 1230–41

[39] Wang D, Zhang M, Chen Z, Li H, Chen A, Wang X and Yang J 2017 Enhanced formaldehyde sensing properties of hollow SnO_2 nanofibers by graphene oxide *Sensors Actuators B* **250** 533–42

[40] Chu X, Zhu X, Dong Y, Zhang W and Bai L 2015 Formaldehyde sensing properties of SnO–graphene composites prepared via hydrothermal method *J. Mater. Sci. Technol.* **31** 913–7

[41] Bo Z, Yuan M, Mao S, Chen X, Yan J and Cen K 2018 Decoration of vertical graphene with tin dioxide nanoparticles for highly sensitive room temperature formaldehyde sensing *Sensors Actuators B* **256** 1011–20

[42] Rong X, Chen D, Qu G, Li T, Zhang R and Sun J 2018 Effects of graphene on the microstructures of SnO_2@rGO nanocomposites and their formaldehyde-sensing performance *Sensors Actuators B* **269** 223–37

[43] Li X, Zhao Y, Wang X, Wang J, Gaskov A M and Akbar S A 2016 Reduced graphene oxide (rGO) decorated TiO_2 microspheres for selective room-temperature gas sensors *Sensors Actuators B* **230** 330–6

[44] Wang Y, Zhou Y and Wang Y 2020 Humidity activated ionic-conduction formaldehyde sensing of reduced graphene oxide decorated nitrogen-doped MXene/titanium dioxide composite film *Sensors Actuators B* **323** 128695

[45] Ye Z, Tai H, Xie T, Yuan Z, Liu C and Jiang Y 2016 Room temperature formaldehyde sensor with enhanced performance based on reduced graphene oxide/titanium dioxide *Sensors Actuators B* **223** 149–56

[46] Mu H, Zhang Z, Zhao X, Liu F, Wang K and Xie H 2014 High sensitive formaldehyde graphene gas sensor modified by atomic layer deposition zinc oxide films *Appl. Phys. Lett.* **105** 033107

[47] Fan J, Li H, Hu H, Niu Y, Hao R, Umar A, Al-Assiri M S, Alsaiari M A and Wang Y 2021 An insight into improvement of room temperature formaldehyde sensitivity for graphene-based gas sensors *Microchem. J.* **160** 105607

[48] Li X, Wang J, Xie D, Xu J, Dai R, Xiang L, Zhu H and Jiang Y 2015 Reduced graphene oxide/hierarchical flower-like zinc oxide hybrid films for room temperature formaldehyde detection *Sensors Actuators B* **221** 1290–8

[49] Sun J, Bai S, Tian Y, Zhao Y, Han N, Luo R, Li D and Chen A 2018 Hybridization of $ZnSnO_3$ and rGO for improvement of formaldehyde sensing properties *Sensors Actuators B* **257** 29–36

[50] Alizadeh T and Soltani L H 2013 Graphene/poly(methyl methacrylate) chemiresistor sensor for formaldehyde odor sensing *J. Hazard. Mater.* **248–249** 401–6

[51] Ding L, Qin Z, Dou Z, Shen Y, Cai Y, Zhang Y and Zhou Y 2018 Morphology-promoted synergistic effects on the sensing properties of polyaniline ultrathin layers on reduced graphene oxide sheets for ammonia and formaldehyde detection *J. Mater. Sci.* **53** 7595–608

[52] Chuang W Y, Yang S Y, Wu W J and Lin C T 2015 A room-temperature operation formaldehyde sensing material printed using blends of reduced graphene oxide and poly (methyl methacrylate) *Sensors* **15** 28842–53

[53] Song L, Luo L, Xi Y, Song J, Wang Y, Yang L, Wang A, Chen Y, Han N and Wang F 2019 Reduced graphene oxide-coated si nanowires for highly sensitive and selective detection of indoor formaldehyde *Nanoscale Res. Lett.* **14** 97

[54] Li X, Wang J, Xie D, Xu J, Xia Y, Xiang L and Komarneni S 2017 Reduced graphene oxide/MoS_2 hybrid films for room-temperature formaldehyde detection *Mater. Lett.* **189** 42–5

[55] Li X, Wang J, Xie D, Xu J, Xia Y, Li W, Xiang L, Li Z, Xu S and Komarneni S 2017 Flexible room-temperature formaldehyde sensors based on rGO film and rGo/MoS_2 hybrid film *Nanotechnology* **28** 325501

[56] Rümmeli M H, Gorantla S, Bachmatiuk A, Phieler J, Geißler N, Ibrahim I, Pang J and Eckert J 2013 On the role of vapor trapping for chemical vapor deposition (CVD) grown graphene over copper *Chem. Mater.* **25** 4861–6

[57] Zhao J, Deng Q, Avdoshenko S M, Fu L, Eckert J and Rummeli M H 2014 Direct *in situ* observations of single Fe atom catalytic processes and anomalous diffusion at graphene edges *Proc. Natl Acad. Sci. USA* **111** 15641–6

[58] Zhao J, Deng Q, Bachmatiuk A, Sandeep G, Popov A, Eckert J and Rummeli M H 2014 Free-standing single-atom-thick iron membranes suspended in graphene pores *Science* **343** 1228–32

[59] Nourbakhsh A, Cantoro M, Klekachev A V, Pourtois G, Vosch T, Hofkens J, van der Veen M H, Heyns M M, De Gendt S and Sels B F 2011 Single layer vs bilayer graphene: a comparative study of the effects of oxygen plasma treatment on their electronic and optical properties *J. Mater. Chem. C* **115** 16619–24

[60] Wu H, Bu X, Deng M, Chen G, Zhang G, Li X, Wang X and Liu W 2019 A gas sensing channel composited with pristine and oxygen plasma-treated graphene *Sensors* **19** 625–7

[61] Feng H, Cheng R, Zhao X, Duan X and Li J 2013 A low-temperature method to produce highly reduced graphene oxide *Nat. Commun.* **4** 1539

[62] Li D W *et al* 2017 Controlled defect creation and removal in graphene and MoS_2 monolayers *Nanoscale* **9** 8997–9008

[63] Ma Z *et al* 2020 Enhanced electrochemical CO_2 reduction of Cu@Cu_xO nanoparticles decorated on 3D vertical graphene with intrinsic sp^3-type defect *Adv. Funct. Mater.* **30** 1910118

[64] Legge E J *et al* 2020 Determining the level and location of functional groups on few-layer graphene and their effect on the mechanical properties of nanocomposites *ACS Appl. Mater. Interfaces* **12** 13481–93

[65] Compagnini G, Giannazzo F, Sonde S, Raineri V and Rimini E 2009 Ion irradiation and defect formation in single layer graphene *Carbon* **47** 3201–7

[66] Eckmann A, Felten A, Mishchenko A, Britnell L, Krupke R, Novoselov K S and Casiraghi C 2012 Probing the nature of

defects in graphene by raman spectroscopy *Nano Lett.* **12** 3925–30
[67] Terrones H, Lv R, Terrones M and Dresselhaus M S 2012 The role of defects and doping in 2D graphene sheets and 1D nanoribbons *Rep. Prog. Phys.* **75** 062501
[68] Kumar S, Tripathi A, Khan S A, Pannu C and Avasthi D K 2014 Radiation stability of graphene under extreme conditions *Appl. Phys. Lett.* **105** 133107
[69] Ferrari A C 2007 Raman spectroscopy of graphene and graphite: disorder, electron–phonon coupling, doping and nonadiabatic effects *Solid State Commun.* **143** 47–57
[70] Casiraghi C, Hartschuh A, Qian H, Piscanec S, Georgi C, Fasoli A, Novoselov K S, Basko D M and Ferrari A C 2009 Raman spectroscopy of graphene edges *Nano Lett.* **9** 1433–41
[71] Cancado L G, Jorio A, Ferreira E H, Stavale F, Achete C A, Capaz R B, Moutinho M V, Lombardo A, Kulmala T S and Ferrari A C 2011 Quantifying defects in graphene via Raman spectroscopy at different excitation energies *Nano Lett.* **11** 3190–6
[72] Kellici S, Acord J, Ball J, Reehal H S, Morgan D and Saha B 2014 A single rapid route for the synthesis of reduced graphene oxide with antibacterial activities *RSC Adv.* **4** 14858
[73] Pham V H, Cuong T V, Hur S H, Oh E, Kim E J, Shin E W and Chung J S 2011 Chemical functionalization of graphene sheets by solvothermal reduction of a graphene oxide suspension in N-methyl-2-pyrrolidone *J. Mater. Chem.* **21** 3371–7
[74] Sinclair R G, McKay A F, Myers G S and Jones R N 2002 The infrared absorption spectra of unsaturated fatty acids and esters1 *J. Am. Chem. Soc.* **74** 2578–85
[75] Kawai T, Umemura J, Takenaka T, Gotou M and Sunamoto J 2002 Fourier transform infrared study on the phase transitions of a 1,2-bis(myristoylamido)-1,2-deoxyphosphatidylcholine-water system *Langmuir* **4** 449–52
[76] Manna B, Raha H, Chakrabarti I and Guha P K 2018 Selective reduction of oxygen functional groups to improve the response characteristics of graphene oxide-based formaldehyde sensor device: a first principle study *IEEE Trans. Electron Devices* **65** 5045–52
[77] Toda K, Furue R and Hayami S 2015 Recent progress in applications of graphene oxide for gas sensing: a review *Anal. Chim. Acta* **878** 43–53
[78] Choi Y R *et al* 2015 Role of oxygen functional groups in graphene oxide for reversible room-temperature NO_2 sensing *Carbon* **91** 178–87
[79] Liu Z, Zhang D, Wei T, Wang L, Li X and Liu B 2019 Adsorption characteristics of formaldehyde on nitrogen doped graphene-based single atom adsorbents: a DFT study *Appl. Surf. Sci.* **493** 1260–7
[80] Cortes-Arriagada D, Villegas-Escobar N, Miranda-Rojas S and Toro-Labbe A 2017 Adsorption/desorption process of formaldehyde onto iron doped graphene: a theoretical exploration from density functional theory calculations *Phys. Chem. Chem. Phys.* **19** 4179–89
[81] Chen X, Xu L, Liu L-L, Zhao L-S, Chen C-P, Zhang Y and Wang X-C 2017 Adsorption of formaldehyde molecule on the pristine and transition metal doped graphene: First-principles study *Appl. Surf. Sci.* **396** 1020–5
[82] Ferrari A C and Basko D M 2013 Raman spectroscopy as a versatile tool for studying the properties of graphene *Nat. Nanotechnol.* **8** 235–46
[83] Ferrari A C *et al* 2006 Raman spectrum of graphene and graphene layers *Phys. Rev. Lett.* **97** 187401
[84] Popov I A, Bozhenko K V and Boldyrev A I 2011 Is graphene aromatic? *Nano Res.* **5** 117–23
[85] Hunt A, Kurmaev E Z and Moewes A 2014 Band gap engineering of graphene oxide by chemical modification *Carbon* **75** 366–71
[86] Luo Z, Shang J, Lim S, Li D, Xiong Q, Shen Z, Lin J and Yu T 2010 Modulating the electronic structures of graphene by controllable hydrogenation *Appl. Phys. Lett.* **97** 233111
[87] Bianco G V, Sacchetti A, Milella A, Grande M, D'Orazio A, Capezzuto P and Bruno G 2020 Extraordinary low sheet resistance of CVD graphene by thionyl chloride chemical doping *Carbon* **170** 75–84
[88] Liu L, Xie D, Wu M, Yang X, Xu Z, Wang W, Bai X and Wang E 2012 Controlled oxidative functionalization of monolayer graphene by water-vapor plasma etching *Carbon* **50** 3039–44
[89] Andre Mkhoyan K, Contryman A W, Silcox J, Stewart D A, Eda G, Mattevi C, Miller S and Chhowalla M 2009 Atomic and electronic structure of graphene-oxide *Nano Lett.* **9** 1058–63
[90] Marsden A J *et al* 2015 Effect of oxygen and nitrogen functionalization on the physical and electronic structure of graphene *Nano Res.* **8** 2620–35
[91] Kim Y H *et al* 2017 Chemically fluorinated graphene oxide for room temperature ammonia detection at ppb levels *J. Mater. Chem. A* **5** 19116–25
[92] Yoosefian M, Raissi H and Mola A 2015 The hybrid of Pd and SWCNT (Pd loaded on SWCNT) as an efficient sensor for the formaldehyde molecule detection: a DFT study *Sensors Actuators B* **212** 55–62
[93] Wang R, Zhang D, Zhang Y and Liu C 2006 Boron-doped carbon nanotubes serving as a novel chemical sensor for formaldehyde *J. Phys. Chem. B* **110** 18267–71
[94] Liang H, Guo L, Cao N, Hu H, Li H, Frans de Rooij N, Umar A, Algarni H, Wang Y and Zhou G 2021 Practical room temperature formaldehyde sensing based on a combination of visible-light activation and dipole modification *J. Mater. Chem. A* **9** 23955–67
[95] Yuan W, Zhang S, Wu Y, Huang X, Tian F, Liu S and Li C 2020 Enhancing the room-temperature catalytic degradation of formaldehyde through constructing surface lewis pairs on carbon-based catalyst *Appl. Catal. B* **272** 118992
[96] Jin Y, Zheng Y, Podkolzin S G and Lee W 2020 Band gap of reduced graphene oxide tuned by controlling functional groups *J. Mater. Chem. C* **8** 4885–94